Wave Motion 89 (2019) 28–42

Contents lists available at ScienceDirect

Wave Motion

journal homepage: www.elsevier.com/locate/wamot

Diffraction by a truncated planar array of dipoles: A Wiener–Hopf approach

Miguel Camacho [a,*], Alastair P. Hibbins [a], Filippo Capolino [b], Matteo Albani [c]

[a] Department of Physics and Astronomy, University of Exeter, Stocker Road, Exeter, United Kingdom
[b] Department of Electrical Engineering and Computer Science, University of California, Irvine, CA 92697, USA
[c] Department of Information Engineering and Mathematics, University of Siena, Siena, Italy

HIGHLIGHTS

- Rigorous, exact analysis for the scattering by a truncated semi-infinite dipole array.
- Rigorous evaluation of diffracted and surface wave currents excited at the array edge.
- Accurate analytical asymptotic formulas are presented showing all wave species.
- Asymptotic analysis vastly reduces computational burden and provides physical insight.
- When supported, the surface wave contribution is often the dominant perturbation.

ARTICLE INFO

Article history:
Received 1 June 2018
Received in revised form 22 January 2019
Accepted 4 March 2019
Available online 7 March 2019

Keywords:
Scattering
Periodic surfaces
Wiener–Hopf
Method of moments
Metasurfaces
Edge diffraction

ABSTRACT

We present a rigorous solution to the problem of scattering of a semi-infinite planar array of dipoles, i.e., infinite in one direction and semi-infinite in the other direction, thus presenting an edge truncation, when illuminated by a plane wave. Such an arrangement represents the canonical problem to investigate the diffraction occurring at the edge-truncation of a planar array. By applying the Wiener–Hopf technique to the Z-transformed system of equations derived from the electric field integral equation, we provide rigorous close form expressions for the dipoles' currents. We find that such currents are represented as the superposition of the infinite array solution plus a perturbation, which comprises both edge diffraction and bound surface waves excited by the edge truncation. Furthermore, we provide an analytical approximation for the double-infinite sum involved in the calculation which drastically reduces the computational effort of this approach and also provides physically-meaningful asymptotics for the diffracted currents.

1. Introduction

The study of the scattering of electromagnetic waves has remained a topic of interest for both physics and engineering communities since the past century. Following the original work of Sommerfeld, who introduced the first theory of diffraction [1], researchers have developed extended theories based on geometrical optics to account for such effects [2,3]. These provide accurate solutions for complex scatterers in terms of closed-form solutions of canonical problems.

* Corresponding author.
E-mail address: mc586@exeter.ac.uk (M. Camacho).

https://doi.org/10.1016/j.wavemoti.2019.03.004

Throughout the development of frequency selective surfaces in the past decade and the subsequent emergence of metasurfaces [4,5], physical optics has allowed for the solution of these periodic problems using the so-called local periodicity approximation to reduce the analysis to a single unit cell with periodic boundary conditions [6,7]. This approximation, although valid in some cases, cannot completely reproduce the behavior of real systems that are finite. It is therefore important to understand the effect that the introduction of truncations have in the response of periodic arrays.

The first studies of scattering arising from array edge truncations dealt with the field radiated by semi-infinite phased arrays, in which the phase and amplitude of the array dipoles were imposed as sources [8–10]. These studies lead to important insights into the radiation and scattering produced by the so called "truncated Floquet waves" and associated diffracted waves at the edge of a semi-infinite array, mainly finding that the field generated by an array-edge truncation possesses several properties analogous to those of the field diffracted by an edge of a half plane [1]. The array-edge diffracted field possesses many spatial harmonics, similarly to the field generated by a periodic grating, however the spatial harmonics of the array-edge diffracted wave have all the same algebraic spreading factor [8,9]. Further studies also explored the scattering of truncated strip arrays [11], and also the double scattering process due to the presence of a truncated ground plane under the truncated array [12]. In [13,14] a method of moments for the currents on a semi-infinite array was constructed using full-domain current basis functions arising from the scattering of edge-truncated array [8,9].

The scattering by large but finite arrays has only been explored using the Method of Moments for the solution of the integral equation involved [15–18]. It was shown that the fields scattered by the truncations can, even in the case of normal incidence, launch surface waves that have greater in-plane momentum than a grazing plane wave, and therefore cannot be excited in an infinite array [19,20]. This is of great importance in various cases, for example when the excitation frequency and wavenumber of the diffracted wave at an array edge is involved in extraordinary optical transmission, in which the collective behavior of the array is responsible for a large resonant transmission through arrayed subwavelength apertures [17,21]. Although some of the previously mentioned studies were able to separate the total diffracted field on the scatterers from that found in the infinite periodic array, they were not able to identify the different contributions to those fields. The effect of these surface waves on finite arrays has been studied in the literature in the context of frequency selective surfaces [22–24].

The existence of surface or leaky waves supported by patterned metallic surfaces, which have been known since the 1940s by the microwave community [25], and the ability to control their radiation have an important role in the design of new generations of antennas [26–29], which take advantage of the high degree of control that metasurfaces allow on their propagation and radiation properties [30–32].

In this paper we provide a rigorous solution to the problem of the scattering of a plane wave that impinges obliquely on a semi-infinite array of dipolar metallic patches using the Wiener–Hopf technique [33,34]. Due to the discrete nature of the problem the Wiener–Hopf method is implemented in the Z-transformed spectral domain for an infinite linear system of equations derived from the electric field integral equation. This technique was previously utilized by some of the authors for the solution of the scattering of a semi-infinite array of metallic strips illuminated by a plane wave [35]. However the semi-infinite planar array of dipoles here considered is periodic in two directions and it has the capability to support bound surface waves that are here specifically investigated. Here we restrict our analysis to the case of a single metallic dipole in each array unit cell, however the obtained description of the wave mechanisms induced by the array-truncation is general, and the same approach could be applied to more general types of truncated planar periodic structures. We need to mention that though the Wiener–Hopf technique applied to the rigorous solution in the Z-transformed domain for discrete current distributions in periodic arrayed structured is rather unusual, there have been important previous contributions [35–43].

2. Integral equation formulation

Let us consider the problem of an arbitrary polarized wave impinging on the semi-infinite planar array of rectangular metallic patches (perfect conducting) whose geometry is depicted in Fig. 1. In the following, a harmonic time dependence $e^{j\omega t}$ is assumed and suppressed throughout the paper. The incident electric field on the plane of the array is written as $\mathbf{E}^{\mathrm{i}} = \mathbf{E}^{\mathrm{i}}_0 \mathrm{e}^{-\mathrm{j}(k_{\mathrm{x}0}x+k_{\mathrm{y}0}y)}$ where $k_{\mathrm{x}0} = k_0 \sin\theta\cos\phi$ and $k_{\mathrm{y}0} = k_0 \sin\theta\sin\phi$, where $k_0 = \omega/c$ is the free space wavenumber and c is the speed of light. The metallic patches are assumed to be perfectly conducting and of negligible thickness. In this case, the tangential component of the electric field on their surface will be zero, leading to the equation

$$\hat{\mathbf{z}} \times \left(\mathbf{E}^{\mathrm{i}}(x,y) + \mathbf{E}^{\mathrm{sc}}(x,y)\right) = \mathbf{0}. \tag{1}$$

In the previous equation, $\mathbf{E}^{\mathrm{sc}}(\mathbf{r})$ represents the electric field scattered by the array due to the impinging plane wave, whose in-plane component can be written in terms of the electric current flowing on the dipoles as

$$\mathbf{E}^{\mathrm{sc}}_{\mathbf{t}}(x,y) = \int_{-\infty}^{\infty}\int_{-\infty}^{\infty} \overline{\mathbf{g}}_{\mathrm{J}}(x-x', y-y') \cdot \mathbf{j}^{\mathrm{sc}}(x',y')\mathrm{d}x'\mathrm{d}y' \tag{2}$$

where $\overline{\mathbf{g}}_{\mathrm{J}}(x-x', y-y')$ is the dyadic Green's function that relates the value of the electric field at (x,y) to that of the surface current at (x',y'). It can be obtained from the discontinuity of the tangential component of the magnetic field,

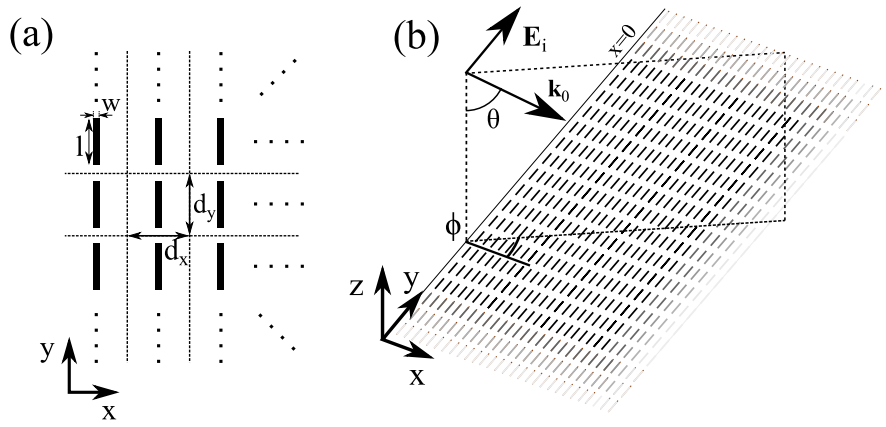

Fig. 1. (a) Top view of the semi-infinite array of polarizable metallic dipoles of length l and width w placed in a rectangular lattice with spacings d_x and d_y along the x and y directions, respectively. (b) Perspective view of the semi-infinite array, truncated at $x = 0$, with incident plane wave.

which can be expressed in terms of the rotational of the electric field via Maxwell's equations. If one substitutes (2) into (1), the result is an integral equation for the currents on the surface of the dipoles $\mathbf{j}^{sc}(x, y)$.

Thanks to the periodicity along the y direction, the problem can be reduced to the analysis of a single strip by introducing the 1-D periodic Green's function such that

$$\mathbf{E}_t^{sc}(x, y) = \int_{-\infty}^{\infty} \int_{-d_y/2}^{d_y/2} \overline{\mathbf{g}}_J^{per}(x - x', y - y') \cdot \mathbf{j}^{sc}(x', y') \mathrm{d}x' \mathrm{d}y' \tag{3}$$

where

$$\overline{\mathbf{g}}_J^{per}(x - x', y - y') = \sum_{m=-\infty}^{\infty} \overline{\mathbf{g}}_J(x - x', y - y' + m d_y) \mathrm{e}^{\mathrm{j}k_{y0} m d_y} \tag{4}$$

Following the reasoning of the Method of Moments (MoM) [44], we will expand the unknown current distribution on each dipole in terms of known functions. We will restrict the following to the use of a single basis function which means a current of the form of $\mathbf{j}_n^{sc}(x, y) = i_n \mathbf{b}_n(x, y)$ where $\mathbf{b}_n(x, y)$ is chosen as

$$\mathbf{b}_n(x, y) = b(x - x_{cn}, y - y_{cn}) \hat{\mathbf{y}} = \frac{\sqrt{1 - \left(\frac{2(y - y_{cn})}{l}\right)^2}}{\sqrt{1 - \left(\frac{2(x - x_{cn})}{w}\right)^2}} \hat{\mathbf{y}} \tag{5}$$

for (x, y) on the surface of the dipole and zero elsewhere, where x_{cn} and y_{cn} are the coordinates of the center of the dipole in the nth unit cell. This first order approximation reproduces the right edge behavior and has been shown to give accurate results at frequencies below the second resonance of the narrow metallic patches [45,46]. This is due to the fact that the square-root reproduces well the behavior of the currents in the proximity of an edge of negligible thickness, leading to a null or to a singularity when the currents are perpendicular or parallel to the edge respectively as shown in Fig. 2.

When the expression for $\mathbf{j}_n^{sc}(x, y)$ is introduced into (3) and then into (1), one can obtain a system of equations for the unknowns i_n by multiplying the resulting expression by the complex conjugate of the basis function associated with the dipole in the mth unit cell, $\mathbf{b}_m^*(x, y)$, and integrating over the surface occupied by such (i.e. Galerkin's version of the MoM [44]) leading to

$$\sum_{n=0}^{\infty} k_{m-n} i_n = v_m \tag{6}$$

where

$$k_{m-n} = \int_{\eta_m} \int_{\eta_n} \mathbf{b}_m^*(x, y) \cdot \overline{\mathbf{g}}_J^{per}(x - x', y - y') \cdot \mathbf{b}_n(x', y') \, \mathrm{d}x\mathrm{d}y \, \mathrm{d}x'\mathrm{d}y' \tag{7}$$

with η_m representing the surface of the mth dipole and where

$$v_m = -\int_{\eta_m} \mathbf{b}_m^*(x, y) \cdot \mathbf{E}_i(x, y) \, \mathrm{d}x\mathrm{d}y = V e^{-\mathrm{j}k_{x0} m d} \tag{8}$$

Due to the fact that the basis functions are non-zero only on the dipoles, the integration domain η_n corresponds to the surface of the nth dipole of the one dimensional semi-infinite chain to which we have reduced the problem. In addition,

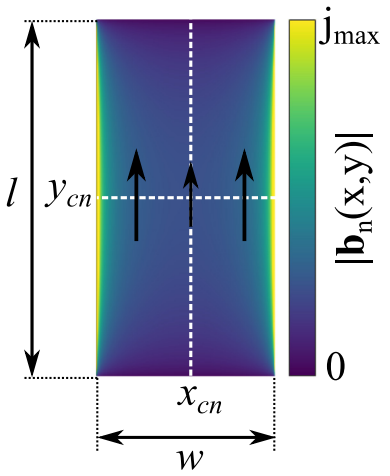

Fig. 2. Current distribution along the $\hat{\mathbf{y}}$ direction of the basis function proposed in Eq. (5). The current diverges at both $x = x_{cn} \pm w/2$ and vanishes at both $y = y_{cn} \pm l/2$ to account for the field distributions in the vicinity of the edges parallel and perpendicular to the direction of the electric current on thin metal patches as shown in [46].

note that the value of k_{m-n} depends on the relative distance between the mth and the nth dipoles and such it has been denoted in terms of the difference between the indexes.

The value of k_{m-n} is obtained in the spectral domain by applying the Fourier transform to the basis functions and the Green's function as

$$k_{m-n} = -\frac{\zeta d_y}{4\pi k_0} \sum_{q=-\infty}^{\infty} \int_{-\infty}^{\infty} \mathrm{d}k_x B(k_x, k_{yq}) B^*(k_x, k_{yq}) \frac{k_0^2 - k_{yq}^2}{\sqrt{k_0^2 - k_x^2 - k_{yq}^2}} e^{-\mathrm{j}k_x(m-n)d_x} \tag{9}$$

where $\zeta = \sqrt{\mu_0/\epsilon_0}$ is the wave impedance of the medium surrounding the array, where $k_{yq} = \frac{2\pi q}{d_y} + k_{y0}$ and where $B(k_x, k_y)$ represents the Fourier transform of the basis function $b(x, y)$ introduced in (5) given by

$$B(k_x, k_{yq}) = \frac{1}{d_y} \int_{-\infty}^{\infty} \int_{-d_y/2}^{d_y/2} b(x - x_{cn}, y - y_{cn}) e^{\mathrm{j}(k_x x + k_{yq} y)} dx dy = \frac{\pi^2 w}{2 k_{yq} d_y} J_1\left(\frac{k_{yq} l}{2}\right) \tag{10}$$

in terms of the first order Bessel function of the first kind $J_1(\cdot)$.

It is important to emphasize that the system of equations shown in Eq. (6) has an infinite number of unknowns (n varies from 0 to ∞). In contrast to introducing a second truncation at a large value of n, we are going to use the Z-transform to solve this system of an infinite number of equations exactly.

A route to solve this problem is to make use of the Z-transform of the successions k_n, i_n and v_n, as the LHS of Eq. (6) is just the convolution of k_n and i_n. The Z-transform of a succession f_n is defined as

$$F(z) = \sum_{n=-\infty}^{\infty} f_n z^{-n} \tag{11}$$

while the inverse Z-transform can be obtained using the expression

$$f_n = \frac{1}{2\pi \mathrm{j}} \int_C F(z) z^{n-1} dz \tag{12}$$

where C denotes a closed counter-clockwise path following the unit circle in the complex z plane. By denoting the Z-transforms of k_n, i_n as $K(z)$ and $I(z)$ respectively we obtain the following equation in the transformed coordinate z

$$K(z) I^+(z) = V \frac{O^-(z)}{O^-(z_\gamma)} \frac{z}{z - z_\gamma} \tag{13}$$

where $z_\gamma = e^{-\mathrm{j}k_{x0}d_x}$, where V was defined in (8) and where the notation $I^+(z)$ indicates that the function is analytical for $|z| > 1$ due to the fact that $i_n = 0$ if $n < 0$ (as naturally follows from (11)). The function $O^-(z)$ is an unknown function with no poles inside the unit circle due to the complex exponential on the RHS of (6) which produces a single pole in the z plane at $z = z_\gamma$.

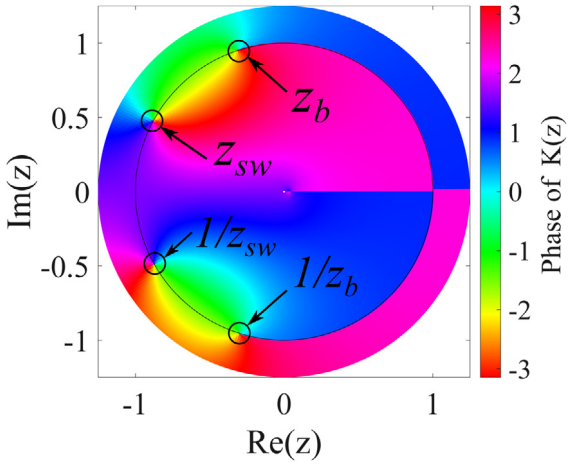

Fig. 3. Plot of the phase of $K(z)$ for the case of $k_{y0} = 0$, $d_x = 0.3\lambda$, $d_y = 0.5\lambda$, $l = 0.3\lambda$ and $w = 0.05\lambda$. The solid line represents the unit circle. The presence of zeros on the second and third quadrant is apparent due to the 2π phase shift around them.

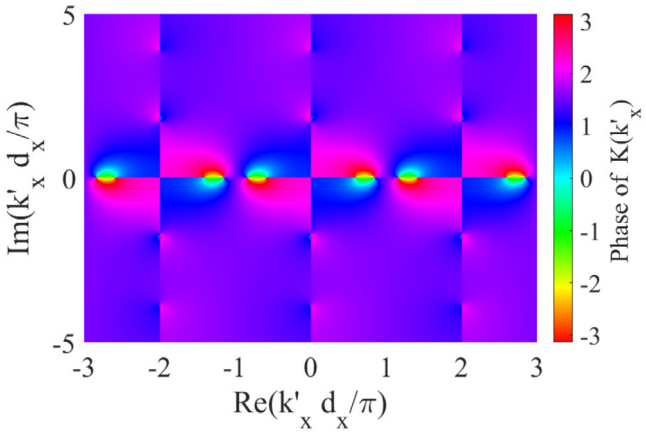

Fig. 4. Plot of $K(k'_x)$ for the case of $k_{y0} = 0$, $d_x = 0.3\lambda$, $d_y = 0.5\lambda$, $l = 0.3\lambda$ and $w = 0.05\lambda$ using the aforementioned conformal transformation.

The value of $K(z)$ can be obtained following (11)

$$K(z) = -\frac{\zeta d_y}{4\pi k_0} \sum_{n=-\infty}^{\infty} z^{-n} \sum_{q=-\infty}^{\infty} \int_{-\infty}^{\infty} \mathrm{d}k_x B(k_x, k_{yq}) B^*(k_x^*, k_{yq}) \cdot \frac{k_0^2 - k_{yq}^2}{\sqrt{k_0^2 - k_x^2 - k_{yq}^2}} e^{-\mathrm{j}k_x n d} \tag{14}$$

By using the conformal mapping $z = \mathrm{e}^{-\mathrm{j}k'_x d_x}$ and the Poisson formula $\sum_{n=-\infty}^{\infty} \mathrm{e}^{-\mathrm{j}(k_x - k'_x)n d_x} = \frac{2\pi}{d_x} \sum_{p=-\infty}^{\infty} \delta(k_x - k'_x - \frac{2\pi p}{d_x})$, (14) can be written as

$$K(z) = -\frac{\zeta d_y}{2 d_x k_0} \sum_{p=-\infty}^{\infty} \sum_{q=-\infty}^{\infty} B\left(k'_x + \frac{2\pi p}{d_x}, k_{yq}\right) B^*\left(k_x'^* + \frac{2\pi p}{d_x}, k_{yq}\right) \cdot \left. \frac{k_0^2 - k_{yq}^2}{\sqrt{k_0^2 - \left(k'_x + \frac{2\pi p}{d_x}\right)^2 - k_{yq}^2}} \right|_{k'_x = \frac{\mathrm{j}}{d_x} \ln z} \tag{15}$$

In Fig. 3, the function $K(z)$ is shown for values of $|z| < 1.25$ in the complex plane obtained from Eq. (15). The branch cuts produced by the square root function accompanied with the singularities associated with the branch points, which will be notated z_b corresponds, in the space of k_x shown in Fig. 4, to $k'_x = \sqrt{k_0^2 - k_{y0}^2}$, located on the real axis (in the lossless case). In the presence of losses, the branches will remain either inside or outside the unit circle. Similarly, in Fig. 4 the values of the function are shown using the conformal mapping introduced earlier in the space of the variable k'_x. The additional branch points due to the terms of the sum with $m, n \neq 0$ are, at frequencies lower than the first diffraction edge, located at purely imaginary values of k'_x, and are mapped onto real values of z with either very small or very large moduli. Thanks to the periodicity of the function in the k'_x plane, only a couple of Riemann sheets (top and bottom) are

found in the z plane. This is on contrast to the many pairs of Riemann sheets that one would found in the k_x' plane, further justifying the reason of performing the Wiener–Hopf technique in the z-domain.

As a new feature with respect to the problem of the scattering by a semi infinite array of strips [35], we find that for the current array problem the function $K(z)$ presents a zero near the branch point. This is due to the fact that two dimensional arrays of dipoles (or slots) support the propagation of surface waves, which are self-supported modes of the system and therefore correspond to zeros of the determinant of the problem [18]. The position of the four points of interest (z_{sw}, $1/z_{sw}$ z_b and $1/z_b$) have been highlighted in Fig. 3.

3. Wiener–Hopf approach

The problems introduced by the presence of the unknown function $O^-(z)$ can be avoided by making use of the factorization of $K(z)$ using the Wiener–Hopf technique, as shown in [35]. If one factorizes $K(z) = K^+(z)K^-(z)$, then (13) is reorganized as

$$\frac{z - z_\gamma}{z} K^+(z) I^+(z) = \frac{O^-(z)}{O^-(z_\gamma)} \frac{V}{K^-(z)} \tag{16}$$

where the factorization is achieved by performing the following integral, which can be derived from applying the sum splitting formula to the logarithm of $K(z)$ [33]

$$K^+(z) = \exp\left[\frac{1}{2\pi \mathrm{j}} \oint_{C_1} \frac{\ln K(s)}{s - z} \mathrm{d}s\right] \tag{17}$$

where C_1 represents the path following the unit circle in the counter-clockwise direction, which has deformed to leave outside the pole at $s = z$. This is a rather complicated integration path, and therefore an alternative expression has been obtained by regularizing the integrand at $s = z$ such that the integral can be performed along the unit circle as

$$K^+(z) = \exp\left[\frac{1}{2\pi \mathrm{j}} \oint_{C} \frac{\frac{1}{2}(1 + \frac{z}{s}) \ln K(s) - \ln K(z)}{s - z} \mathrm{d}s\right] \tag{18}$$

Then, according to Liouville's theorem, if a function is bound and analytic everywhere on the complex plane then it is a constant. In the problem studied here, the limit $|z| \to \infty$ corresponds with $\mathrm{Im}\, k_x' \to +\infty$, for which the function $K(z)$ decays to zero given that its only dependence on k_x' is contained in the square root denominator, and therefore also $K^+(z)$ and the LHS of (16). This constant can be easily obtained by evaluating the RHS of (16) at $z = z_\gamma$, obtaining the Z-transformed current as

$$I^+(z) = I(z) = \frac{V}{K^+(z)K^-(z_\gamma)} \frac{z}{z - z_\gamma} \tag{19}$$

from which the value of i_n can be obtained through the inverse Z-transform as

$$i_n = \frac{V}{2\pi \mathrm{j}} \frac{1}{K^-(z_\gamma)} \oint_C \frac{1}{K^+(z)} \frac{z^n}{z - z_\gamma} \mathrm{d}z \tag{20}$$

where C corresponds to an integration path around the unit circle as shown in Fig. 5.

From Figs. 3 and 4 and Eq. (20), one can see that the currents on the each dipole will have three contributions

$$i_n = i_n^\infty + i_n^d + i_n^{\mathrm{sw}} \tag{21}$$

which arise from the different poles and branch cuts found inside the unit circle, shown in Fig. 5. The total current on the dipoles has been found to be given by the sum of those found in the non-truncated array plus a surface wave contribution (associated with the pole z_{sw}) plus the currents generated by the continuous spectrum of the edge-diffraction, which mathematically correspond to

$$i_n^\infty = V \frac{\mathrm{e}^{-\mathrm{j}k_{x0} n d_x}}{K(z_\gamma)} \tag{22}$$

$$i_n^{sw} = \frac{V}{2\pi \mathrm{j}} \frac{1}{K^-(z_\gamma)} \oint_{C_{\mathrm{sw}}} \frac{1}{K^+(z)} \frac{z^n}{z - z_\gamma} \mathrm{d}z = \frac{V}{2\pi \mathrm{j}} \frac{\mathrm{e}^{-\mathrm{j}k_{x0}^{\mathrm{sw}} n d_x}}{K^-(z_\gamma)} \lim_{z \to z_{sw}} \frac{1}{K^+(z)} \frac{z - z_{\mathrm{sw}}}{z - z_\gamma} \tag{23}$$

and

$$i_n^d = \frac{V}{2\pi \mathrm{j}} \frac{1}{K^-(z_\gamma)} \oint_{C_b} \frac{1}{K^+(z)} \frac{z^n}{z - z_\gamma} \mathrm{d}z \tag{24}$$

Eqs. (15) to (23) constitute the closed-form solution of the diffraction current by a semi-infinite array of dipoles under plane-wave illumination. This solution, although exact within the single basis function approximation, suffers from the

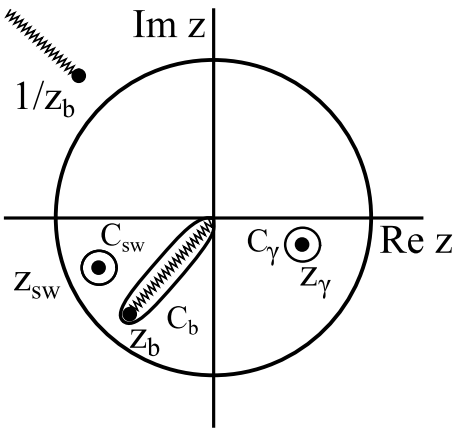

Fig. 5. Unit circle of integration C in the z-domain to perform the inverse Z-transform (20). The C integration path in (20) is deformed onto three integration paths around the singularities leading to three distinct wave species: (1) the contour around the pole z_{sw} corresponds to the current i_n^{sw} associated to the surface wave; (2) the contour around the branch cut represents the continuous spectrum of the diffracted current i_n^{d} that will be asymptotically evaluated in the last part of this paper; and (3) the contour around the pole z_γ provides the current i_n^{∞} pertaining to the infinite array (without truncation) due to plane wave excitation. The branch cut locus has been modified as a straight line to simplify the calculation of the contour integral since this is associated to a steepest descent path as shown in [35].

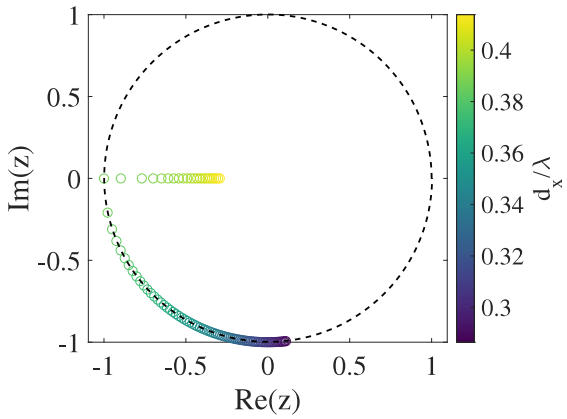

Fig. 6. Map of the position of the zeros of $K(z)$ (z_{sw}) for different values of the normalized frequency d_x/λ for a fix value of $d_y = 4/3d_x$, $l = d_x$, $w = d_x/30$ and $\alpha = 0$ found using the iterative zero search algorithm in [52].

need to calculate numerically integrals of slowly convergent two dimensional infinite series as shown in (18) and (15). In addition, the position of the poles corresponding to the existence of surface waves need to be found numerically for each set of parameters as they move as shown in Fig. 6, requiring an additional number of evaluations of the integrand. Several methods have been proposed to reduce the computational effort needed to compute the two-dimensional infinite series, which appears in the solution of the infinite two-dimensional periodic array of dipoles [47]. However, the most effective has been shown to be the calculation of the matrix elements in the spatial domain, which in addition to the advantages from using the Ewald's method [48–50] for the computation of the two-dimensional periodic Green's function leads to the calculation of finite-domain integrals [17,51].

To facilitate the numerical calculation of the contribution of the currents arising from diffraction, it is convenient to introduce the change of variable $z = z_b \mathrm{e}^{-s^2}$ such that the integral in (24) becomes

$$i_n^d = -\frac{V}{\pi \mathrm{j}} \frac{z_b^{n+1}}{K(z_\gamma)} \int_{-\infty}^{\infty} \left[\frac{K^+(z_\gamma)}{K^+(z_b \mathrm{e}^{-s^2})} \right] \frac{s\, \mathrm{e}^{-(n+1)s^2}}{z_b \mathrm{e}^{-s^2} - z_\gamma} \mathrm{d}s = -\frac{V}{\pi \mathrm{j}} \frac{z_b^{n+1}}{K(z_\gamma)} \int_{-\infty}^{\infty} F_n(s) \mathrm{d}s \tag{25}$$

where the integrand is calculated on each side of the branch cut for $s < 0$ and $s > 0$ respectively. As shown in [35], this expression is also more suitable for asymptotic analysis.

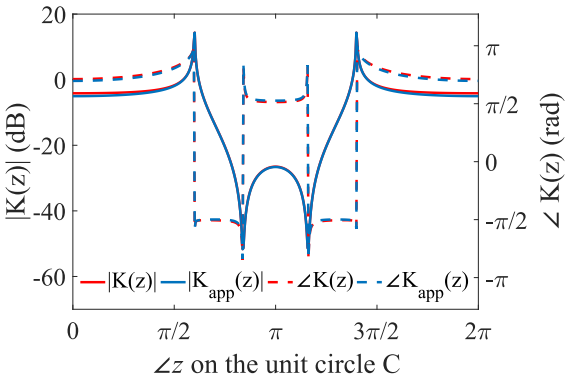

Fig. 7. Map of the amplitude and phase of the exact and approximated $K(z)$ function for points on the unit circle. The zeros are introduced into the approximation by applying a zero-search algorithm to the exact form.

4. Approximate factorization

To avoid the computational effort required to calculate the function $K^+(z)$ using Eq. (18), we propose an approximate factorization $K(z) \approx K^+_{\text{app}}(z)K^-_{\text{app}}(z)$ based on the main term of Eq. (15) given, when the array supports a surface wave with wavevector k_x^{sw} such that $z_{sw} = \mathrm{e}^{-\mathrm{j}k_x^{sw}d_x}$, by

$$K^+_{\text{app}}(z) = A\left(\frac{D}{\sqrt{1-z_b/z}} + C\right)\frac{z - z_{sw}}{z_b - z_{sw}}\frac{z_b - z_{sw}^{\text{app}}}{z - z_{sw}^{\text{app}}} \tag{26}$$

$$K^-_{\text{app}}(z) = A\left(\frac{D}{\sqrt{1-z_b z}} + C\right)\frac{1/z - z_{sw}}{1/z_b - z_{sw}}\frac{1/z_b - z_{sw}^{\text{app}}}{1/z - z_{sw}^{\text{app}}} \tag{27}$$

where the constants A, C and D are given by

$$A = \left(\frac{D}{\sqrt{1-z_b^2}} + C\right)^{-1/2} \tag{28}$$

$$D = \lim_{z\to z_b} K(z)\sqrt{1-z_b/z} = -\frac{\zeta\sqrt{\mathrm{j}d_y}}{2\sqrt{2d_x k_b}k_0}B(k_b, k_{y0})B^*(k_b^*, k_{y0})(k_0^2 - k_{y0}^2) \tag{29}$$

and

$$C = \lim_{z\to z_b} K(z) - \frac{D}{\sqrt{1-z_b/z}} = -\frac{\zeta\, d_y}{2d_x k_0}\sum_{p\neq 0}\sum_{q\neq 0} B\left(k_b + \frac{2\pi p}{d_x}, k_{yq}\right)\cdot B^*\left(k_b^* + \frac{2\pi p}{d_x}, k_{yq}\right)\cdot\frac{k_0^2 - k_{yq}^2}{\sqrt{k_0^2 - \left(k_b + \frac{2\pi p}{d_x}\right)^2 - k_{yq}^2}} \tag{30}$$

These expressions have been obtained by studying the limit of $K(k_x')$ when k_x' approaches $k_b = \sqrt{k_0^2 - k_{y0}^2}$, whose behavior is dominated by the $p = q = 0$ element of the series in (15), and whose branch cut is preserved by the approximation. The remaining terms vary slowly in the neighborhood of the branch point k_b and can be therefore approximated as a constant (C) as shown in (26) and (27). In the limit, the proposed approximated function reproduces the behavior of the original $K(z)$ function and allows for the analytical asymptotic study of the diffracted currents. It should be mentioned that the first two factors in (26) and (27) are completely analogous to the expansion presented in [35], and the two additional factors have been introduced to account for the existence of surface waves at $z = z_{sw}$, which can be added without impacting the behavior of the functions for $|z| \to \infty$ by removing the non-physical zero at $z_{sw}^{\text{app}} = z_b/(1 - (D/C)^2)$. The value of z_{sw}, however, needs to be obtained using the exact expression for $K(z)$ using an iterative procedure based on [52]. In Fig. 7 we map the values of the modulus and phase of the exact and approximated $K(z)$ functions given by (15) and (26) respectively for points on the unit circle, showing an excellent agreement. There, the presence of the branch points $z = z_b$ and $z = 1/z_b$ and the zeros $z = z_{sw}$ and $z = 1/z_{sw}$ of the $K(z)$ functions can be observed. In addition, to show the validity of the approximation for its use on the calculation of (25), the value of the exact and approximated integrands for the first dipole are shown in Fig. 8.

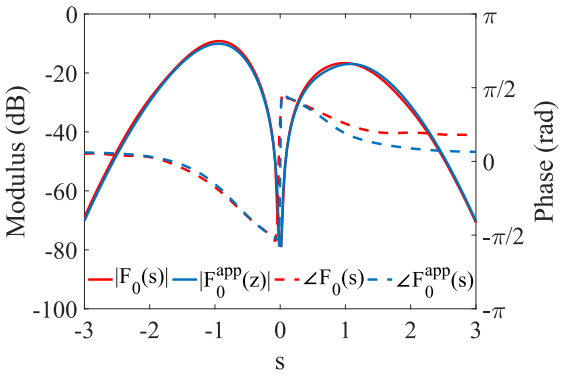

Fig. 8. Map of the modulus and phase of the exact and approximated integrand $F_n(s)$ in (25) and $F_n^{\text{app}}(s)$ in (32), making use of the exact and approximated factorizations of $K(z)$.

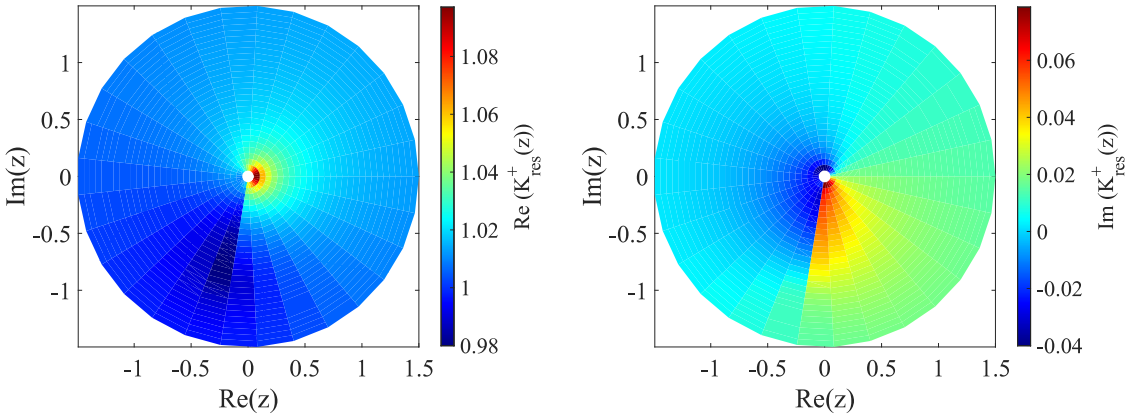

Fig. 9. Plot of $K_{\text{res}}^{+}(z)$ for $|z| \leq 1.5$ for the case of $d_x = 0.3\lambda$, $d_y = 0.4\lambda$, $l = 0.3\lambda$ and $w = 0.01\lambda$ computed numerically. In this case, the array does not support any surface wave and the terms associated with them are removed from the approximation.

Note that for the cases in which the chosen geometrical parameters do not lead to the existence of a surface wave solution (such as small dipole lengths with respect to the periodicity), the formulas presented in [35] should be used instead, making use of the constants here presented. This just means to remove the factors including z_{sw} and z_{sw}^{app}. Under these circumstances the diffracted currents are those arising from the fields diffracted by the truncation. In this case, we have checked the validity of the approximation through the calculation of $K_{\text{res}}^{+}(z) = K^{+}(z)/K_{\text{app}}^{+}(z)$ (such that $K_{\text{res}}(z) = K(z)/K_{\text{app}}(z)$), given analogously to (18) by

$$K_{\text{res}}^{+}(z) = \exp\left[\frac{1}{2\pi \text{j}} \oint_C \frac{\frac{1}{2}(1+\frac{z}{s})\ln K_{\text{res}}(s) - \ln K_{\text{res}}(z)}{s-z} \text{d}s\right] \tag{31}$$

In Fig. 9, the real and imaginary parts of the function $K_{\text{res}}^{+}(z)$, obtained using (31), have been plotted. The integral was performed numerically by introducing small losses in the system so that the branch points were located slightly inside and outside of the unit circle, removing numerical instabilities. In addition, due to the different locations of the branch cuts of the expressions (15) and (26), the definition of the branch cut of the term $m, n = 0$ in (15) was modified so that it became radial.

As the reader can see, the real part is very close to one everywhere with the exception of where those additional branch cuts are found, but still the correction is smaller than ten percent. The imaginary part is also found to be very close to zero, with very small deviations near the branch cut.

This approximate factorization has been shown to be very accurate in the proximity of the branch cut, as shown later in the results section, regardless of the existence of surface waves, and allows for a vast reduction in the computation time needed for the calculation of the branch contribution, i_n^d, in terms of the diffracted fields.

5. Asymptotic evaluation of the diffracted currents

Among the different contributions to the total current, that representing the diffracted current is the most computationally demanding, as it requires the integration of the function $K^+(z)$, which is itself calculated through the integral of a very slowly convergent function, as mentioned earlier. It is therefore convenient to obtain an asymptotic approximation for i_n^d, which is obtained thanks to the approximated factorization presented in the previous section. The approximate form of the diffracted current is hence given by

$$i_n^d \approx -\frac{V}{\pi \mathrm{j}} \frac{z_b^{n+1}}{K(z_\gamma)} \int_{-\infty}^{\infty} \left[\frac{K_{\mathrm{app}}^+(z_\gamma)}{K_{\mathrm{app}}^+(z_b \mathrm{e}^{-s^2})} \right] \frac{s\, \mathrm{e}^{-(n+1)s^2}}{z_b \mathrm{e}^{-s^2} - z_\gamma} \mathrm{d}s = -\frac{V}{\pi \mathrm{j}} \frac{z_b^{n+1}}{K(z_\gamma)} \int_{-\infty}^{\infty} F_n^{\mathrm{app}}(s) \mathrm{d}s \tag{32}$$

Thanks to the exponential decay of the integrand, the value of the integral is dominated by small values of s. The factor involving the function $K_{\mathrm{app}}^+(z)$ is approximated as

$$\frac{K_{\mathrm{app}}^+(z_\gamma)}{K_{\mathrm{app}}^+(z_b \mathrm{e}^{-s^2})} \approx \mathrm{j}sD^{-1} \left(\frac{D}{\sqrt{1 - z_b/z_\gamma}} + C \right) \frac{z_\gamma - z_{sw}}{z_b - z_{sw}} \frac{z_b - z_{sw}^{\mathrm{app}}}{z_\gamma - z_{sw}^{\mathrm{app}}} \tag{33}$$

which then reduces to the following integral

$$i_n^d \approx -\frac{V}{\pi} \frac{z_b^{n+1}}{K(z_\gamma) D} \left(\frac{D}{\sqrt{1 - z_b/z_\gamma}} + C \right) \frac{z_\gamma - z_{sw}}{z_b - z_{sw}} \frac{z_b - z_{sw}^{\mathrm{app}}}{z_\gamma - z_{sw}^{\mathrm{app}}} \int_{-\infty}^{\infty} \frac{s^2\, \mathrm{e}^{-(n+1)s^2}}{z_b \mathrm{e}^{-s^2} - z_\gamma} \mathrm{d}s \tag{34}$$

When poles are not in the "vicinity" (in the asymptotic sense) of the branch point in the z domain (poles not close to the saddle point at $s = 0$ in the s domain, this integral is accurately evaluated in a non-uniform asymptotic fashion as in [35] leading to

$$i_n^d \approx \frac{\mathrm{e}^{-\mathrm{j}\sqrt{k_0^2 - k_{y0}^2}(n+1)d_x}}{(n+1)^{3/2}} \frac{R^d}{z_b - z_\gamma}, \tag{35}$$

where

$$R^d = -\frac{V}{2\sqrt{\pi} D K(z_\gamma)} \left(\frac{D}{\sqrt{1 - z_b/z_\gamma}} + C \right) \frac{z_\gamma - z_{sw}}{z_b - z_{sw}} \frac{z_b - z_{sw}^{\mathrm{app}}}{z_\gamma - z_{sw}^{\mathrm{app}}}. \tag{36}$$

The asymptotic expression (35) for the diffracted current reveals that it corresponds to the current induced by an edge-diffracted wave which has a cylindrical wavefront with an amplitude spreading (unlike the infinite-array and surface-wave currents which have no spreading) that decays as $1/(n+1)^{3/2}$ from the truncation of the array at $x = 0$.

6. Illustrative examples

In this section we explore the physics behind the excitation of the diffracted field and, in some cases, the conversion of free space radiation into surface-bound propagative waves along the array surface.

Let us start by considering the case of small metallic patches compared to the periodicity. This system does not support long wavelength (when compared to the periodicity) propagation of surface modes as these appear at frequencies near their resonance and therefore the only contributions arise from the diffracted fields and the solution of the infinite periodic problem, i.e., $i_n = i_n^\infty + i_n^d$ which are calculated using the exact Eqs. (22) and (25). The calculated total normalized current for the first 30 elements along the x direction are shown in Fig. 10. The current obtained by the Wiener–Hopf method is compared to that obtained from a method of moments solution of the scattering by a finite-by-infinite array, i.e., the array is finite along the x direction with 2000 unit cells, enough for the diffracted fields to decay so that edge-induced diffracted fields do not interact with each other. These two solutions are in excellent agreement, and show the small magnitude of the diffracted currents, about three orders of magnitude smaller than the currents in infinite array. In addition, we show the validity of the solution obtained using the approximated factorization, which leads to an accurate semi-analytical solution calculated via (32) in contrast to the very computationally expensive numerical factorization using (18), needed for the computation of (25).

In a second example we increase the length of the metallic patches and reduce their spacing along the x direction in terms of the wavelength, so that the coupling between the dipoles is increased, leading to the existence of self-supported current solutions that propagate along the array. These modal solutions can be computed by finding the zeros of the determinant of the matrix of the linear system of equations obtained for the scattering by an infinite two-dimensional array of dipoles, which is actually proportional to the $K(z)$ function as it can by shown by direct comparison with [18] and [53]. These solutions are characterized by their in-plane wavevector $(k_{x0}^{\mathrm{sw}}, k_{y0}^{\mathrm{sw}})$ at each frequency. In Fig. 11 the value of the determinant of the scattering problem by a double infinite periodic array of dipoles is shown for different in-plane wavevector in dB scale. The minima (in blue) correspond to the in-plane wavevectors of the surface waves supported by

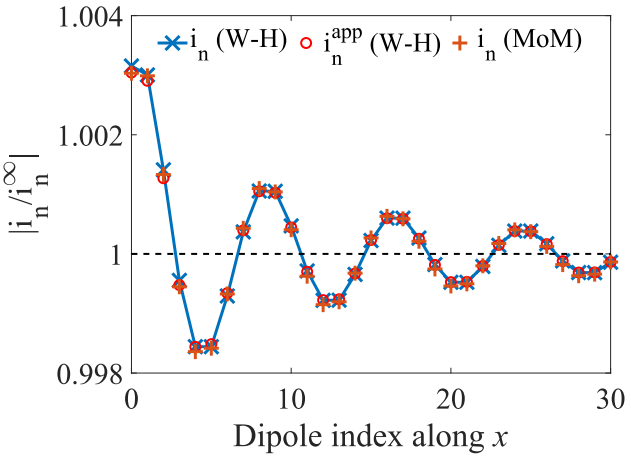

Fig. 10. Total current i_n obtained with the discrete Wiener–Hopf method normalized to i_n^{∞} on the first 30 dipoles away from the $x = 0$ truncation of a semi-infinite array with $d_x = 0.125\lambda$, $d_y = 0.125\lambda$, $l = 0.05\lambda$ and $w = 0.0125\lambda$. The current i_n is calculated via (25). In this case the arrays does not support surface waves, hence $i_n^{\text{sw}} = 0$. The result is in excellent agreement with that obtained from a method of moment for the scattering by a finite-by-infinite array with by a 2000 unit cells in the x direction. Red circles represent the currents obtained using the approximated factorization presented in Section 4 with an excellent agreement.

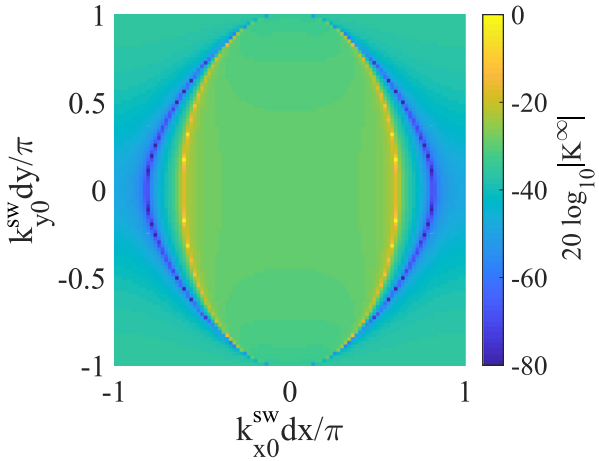

Fig. 11. Isofrequency map of the determinant of the system of equations arising from the solution of the scattering by a doubly infinite periodic array of dipoles for the case of $d_x = 0.3\lambda$, $d_y = 0.5\lambda$, $l = 0.4\lambda$ and $w = 0.05\lambda$.

the array at this wavelength while the maxima (in yellow) represent the light cone, due to the divergence of the periodic Green's function at grazing incidence [53]. When the light circle is large enough that it crosses the Brillouin zone boundary, this divergence can be noticed in the frequency-dependent transmission coefficient through the array as a sharp null. This is commonly known as the Wood's anomaly, and is responsible for the well-known extraordinary transmission effect at microwave frequencies [54].

Thanks to the introduction of a truncation parallel to the y direction, the scattered fields present a continuous spectrum in k_x and a discrete spectrum in k_y direction. Surface waves satisfy $k_{x0}^{\text{sw}} > k_0$ and $k_{y0}^{\text{sw}} = k_{y0}$ which means that one could, by tilting the angle of incidence on the $y-z$ plane excite all the surface waves with the same in-plane wavevector as the impinging wave along the y direction shown in Fig. 11. This means that, one can access all spectral components defined by the line $k_{y0}^{\text{sw}} = k_{y0}$, regardless of the value of k_{x0}^{sw}, in contrast to the non-truncated problem, for which one cannot access the non-visible range defined by $k_{x0}^{\text{sw}} > k_0$ when $k_0 < \pi/d_x$. Thanks to the symmetry of the system presented here, this isofrequency map is symmetric with respect to the $k_{x0}^{\text{sw}} = 0$ and $k_{y0}^{\text{sw}} = 0$ planes. This symmetry means that, in the z plane, both z_{sw} and $1/z_{sw}$ are zeros of $K(z)$.

At normal incidence ($k_{y0} = 0$), two modes are symmetrically found with $k_{x0}^{\text{sw}} \approx \pm 1.35 k_0$, which correspond to two poles in the Z-plane (one being the inverse of the other). In the absence of losses will be located on the unit circle as shown in Fig. 12. Therefore, one could assume that both surface waves could be excited by the diffracted fields due to Eq. (23), but actually only one of those two waves correspond to a physical solution of the problem, as the truncation cannot excite

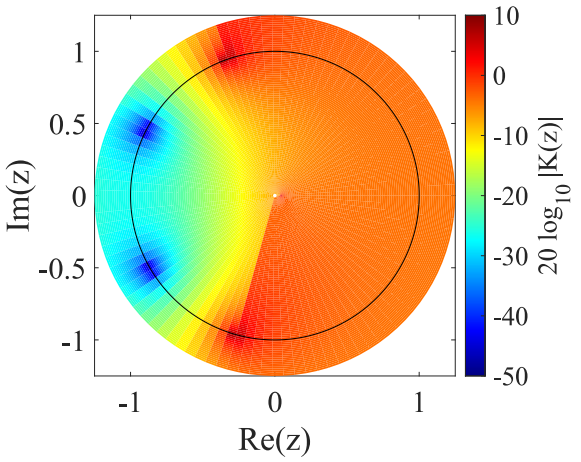

Fig. 12. Map of the magnitude of $K(z)$ for the case of $k_{y0} = 0$, $d_x = 0.3\lambda$, $d_y = 0.5\lambda$, $l = 0.\lambda$ and $w = 0.05\lambda$. The solid line represents the unit circle.

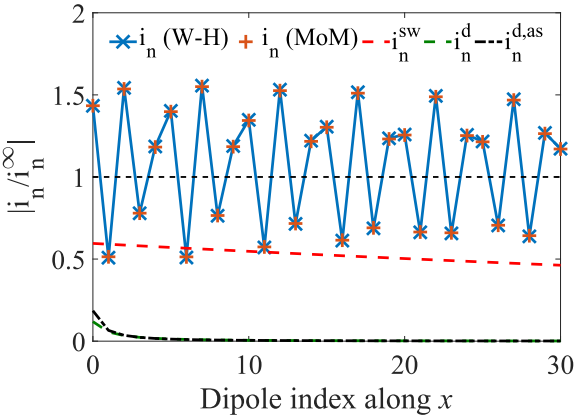

Fig. 13. Total current i_n obtained with the discrete Wiener–Hopf method, and the two current contributions i_n^d, and i_n^{sw} in (21), normalized to i_n^{∞}, on the first 30 dipoles away from the $x = 0$ truncation of a semi-infinite array with $d_x = 0.3\lambda$, $d_y = 0.5\lambda$, $l = 0.3\lambda$ and $w = 0.05\lambda$. Currents i_n, i_n^{sw}, and i_n^d are calculated via (21), (23), and (25), respectively. The current solution obtained from a method of moments for a finite-by-infinite array of 2000 cells in the x direction is also included for comparison. The black dash-dotted line represents the analytical asymptotic approximation of the diffracted currents $i_n^{d,\mathrm{as}}$ calculated via (35), whereas the green-dashed line represents the exact i_n^d calculated via (25) . (For interpretation of the references to color in this figure legend, the reader is referred to the web version of this article.)

a wave that propagates energy towards the edge itself (i.e. with a x component of the group velocity that is negative). Mathematically this can be proved by introducing small losses into the system, which make the two poles displace, one towards the inner part of the circle and the other towards the outer part, therefore not contributing to the closed path integral of (20).

In Fig. 13, we show the Wiener–Hopf solution of the scattering by the truncation for the case of normal incidence shown in previous figures, in which the array supports a pair of symmetric surface waves, although the truncation is only able to excite the surface wave that propagates towards the positive x direction. By comparing the Figs. 10 and 13, the currents introduced by the excitation of the surface wave have large magnitude, more than half of that of the currents in the infinite array. These surface wave currents are responsible for long-range effects, decaying only due to small losses (loss tangent of 10^{-6}) that were introduced to make the validation against the 2000 cell finite-by-infinite method of moments feasible. Due to the large amplitude of the surface wave, the diffracted currents constitute a second order perturbation to the periodic solution. Nonetheless, they can be very accurately calculated using the analytical approximated factorization, and also by using the analytical asymptotics as shown in the figure. The exact currents i_n, i_n^{sw}, and i_n^d and the asymptotic diffracted currents $i_n^{\mathrm{d,as}}$ are calculated using (21), (23), (25), and (35), respectively.

We have also explored the dependence of the excited currents on the angle of incidence when the impinging wavevector is parallel to the x-z plane. When k_{y0} is kept as a constant, the function $K(z)$ does not vary with the angle of incidence as shown in Eq. (15) and therefore only the value of V and z_γ will vary with the angle. In Fig. 14 we show the total normalized currents excited on the dipoles for $\theta = 0$ and $\theta = \pi/4$ with $\phi = 0$ and $\phi = \pi$. The figure shows a large enhancement of the surface currents as the x component of the impinging wavevector has the same sign of

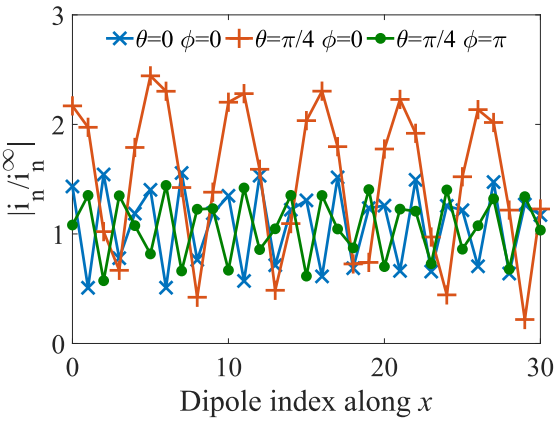

Fig. 14. Normalized total current i_n obtained with the discrete Wiener–Hopf method for the same semi-infinite array as in Fig. 13, for different angles of incidence on the $x-z$ plane.

that of the surface wave, these being in magnitude more than twice those expected for the infinite array. In contrast, when the impinging wavevector points along the negative x direction, the excited surface wave currents do not present a large variation with respect to normal incidence. Due to the resonant nature of the surface waves, this large variation of amplitude with the spectral component of the diffracted fields that matches that of the surface waves is to be expected.

7. Conclusions

We have presented a rigorous analysis of the scattering by a semi-infinite array of dipoles using the Wiener–Hopf technique in the Z-transformed domain due to the discrete nature of the planar current distribution. This method provides us with a physical insight into the currents on the semi-infinite array upon plane wave excitation, by providing an exact representation based on the single assumption that the current shape on each array elements is fixed, i.e., each array element responds to the field as a dipolar current with prescribed shape. The total current on the array is exactly represented in terms of three wave species, the one that would exist on the infinite array without any truncation plus two other wave contributions that arise from the array-truncation: the continuous spectrum forming the diffracted fields arising from the edge truncation of the array and algebraically decaying with the edge distance and the excited surface wave propagating along the array surface, also excited by the array edge-truncation, that propagates along the whole semi-infinite array. This paper constitutes the first fully-theoretical prediction with closed form formulas rigorously obtained for a semi-infinite array of metallic dipoles, not based on full-wave numerical solutions. Note that the wave species obtained in this paper are also have also a physical meaning when the array has a finite width $L = Nd_x$, with N the total number or unit cells in the x direction, as long as the two array-edges are "far away" from each other, since diffracted waves decay algebraically away from the two edges. Here with "far away" we mean that $(\lambda/L)^{3/2} \ll 1$ because the algebraic decay is in the form of $1/(nd_x)^{3/2}$, with the array edge at $x = 0$, so that the current diffracted by one edge is negligible at the other edge. An outcome of this method is that the interaction of surface waves at the two array-edges could also be studied.

Acknowledgment

The authors wish to acknowledge financial support from the Engineering and Physical Sciences Research Council (EPSRC) of the United Kingdom, via the EPSRC Centre for Doctoral Training in Metamaterials (Grant No. EP/L015331/1). All data created during this research are openly available from the University of Exeter's institutional repository at https://ore.exeter.ac.uk/.

References

[1] A. Sommerfeld, Mathematische theorie der diffraction. (mit einer tafel), Math. Ann. 47 (1896) 317–374, URL http://eudml.org/doc/157794.
[2] J.B. Keller, A geometrical theory of diffraction, J. Opt. Soc. Amer. 52 (2) (1962) 116–130, http://dx.doi.org/10.1364/JOSA.52.000116, URL https://www.osapublishing.org/abstract.cfm?URI=josa-52-2-116.
[3] R.G. Kouyoumjian, P.H. Pathak, A uniform geometrical theory of diffraction for an edge in a perfectly conducting surface, Proc. IEEE 62 (11) (1974) 1448–1461, http://dx.doi.org/10.1109/PROC.1974.9651, URL http://ieeexplore.ieee.org/lpdocs/epic03/wrapper.htm?arnumber=1451581.
[4] B.A. Munk, Frequency Selective Surfaces: Theory and Design, 2000, p. 410, URL https://www.wiley.com/en-gb/Frequency+Selective+Surfaces%3A+Theory+and+Design-p-9780471370475.
[5] N. Yu, F. Capasso, Flat optics with designer metasurfaces, Nature Mater. 13 (2) (2014) 139–150, http://dx.doi.org/10.1038/nmat3839, URL http://www.nature.com/doifinder/10.1038/nmat3839.

[6] G. Minatti, F. Caminita, E. Martini, M. Sabbadini, S. Maci, Synthesis of modulated-metasurface antennas with amplitude, phase, and polarization control, IEEE Trans. Antennas Propag. 64 (9) (2016) 3907–3919, http://dx.doi.org/10.1109/TAP.2016.2589969, URL http://ieeexplore.ieee.org/document/7508983/.

[7] R. Florencio, R.R. Boix, J.A. Encinar, G. Toso, Optimized periodic MoM for the analysis and design of dual polarization multilayered reflectarray antennas made of dipoles, IEEE Trans. Antennas and Propagation 65 (7) (2017) 3623–3637, http://dx.doi.org/10.1109/TAP.2017.2702700, URL http://ieeexplore.ieee.org/document/7922490/.

[8] F. Capolino, M. Albani, S. Maci, L.B. Felsen, Frequency-domain green's function for a planar periodic semi-infinite phased array-part I: Truncated floquet wave formulation, IEEE Trans. Antennas and Propagation 48 (1) (2000) 67–74, http://dx.doi.org/10.1109/8.827387, URL http://ieeexplore.ieee.org/document/827387/.

[9] F. Capolino, M. Albani, S. Maci, L.B. Felsen, Frequency-domain Green's function for a planar periodic semi-infinite phased array - Part II: Diffracted wave phenomenology, IEEE Trans. Antennas and Propagation 48 (1) (2000) 75–85, http://dx.doi.org/10.1109/8.827388.

[10] F. Capolino, L.B. Felsen, Short-pulse radiation by a sequentially excited semi-infinite periodic planar array of dipoles, Radio Sci. 38 (2) (2003) http://dx.doi.org/10.1029/2001rs002588, n/a–n/a.

[11] L. Carin, L.B. Felsen, Time harmonic and transient scattering by finite periodic flat strip arrays: Hybrid (ray)-(floquet mode)-(MOM) algorithm, IEEE Trans. Antennas and Propagation 41 (4) (1993) 412–421, http://dx.doi.org/10.1109/8.220973, URL http://ieeexplore.ieee.org/document/220973/.

[12] F. Capolino, M. Albani, S. Maci, R. Tiberio, High-frequency analysis of an array of line sources on a truncated ground plane, IEEE Trans. Antennas and Propagation 46 (4) (1998) 570–578, http://dx.doi.org/10.1109/8.664123, URL http://ieeexplore.ieee.org/document/664123/.

[13] A. Neto, S. Maci, G. Vecchi, M. Sabbadini, A truncated Floquet wave diffraction method for the full wave analysis of large phased arrays-part I: Basic principles and 2-D cases, IEEE Trans. Antennas and Propagation 48 (4) (2000) 594–600, http://dx.doi.org/10.1109/8.843674, URL http://ieeexplore.ieee.org/document/843674/.

[14] A. Neto, S. Maci, G. Vecchi, M. Sabbadini, A truncated Floquet wave diffraction method for the full-wave analysis of large phased arrays-part II: Generalization to 3-D cases, IEEE Trans. Antennas and Propagation 48 (4) (2000) 601–611, http://dx.doi.org/10.1109/8.843675, URL http://ieeexplore.ieee.org/document/843675/.

[15] Ö.A. Çivi, P.H. Pathak, H.T. Chou, P. Nepa, Hybrid uniform geometrical theory of diffraction - moment method for efficient analysis of electromagnetic radiation/scattering from large finite planar arrays, Radio Sci. 35 (2) (2000) 607–620, http://dx.doi.org/10.1029/1999RS001922, URL http://doi.wiley.com/10.1029/1999RS001922.

[16] C. Craeye, A.G. Tijhuis, D.H. Schaubert, An efficient MoM formulation for finite-by-infinite arrays of two-dimensional antennas arranged in a three-dimensional structure, IEEE Trans. Antennas and Propagation 52 (1) (2004) 271–282, http://dx.doi.org/10.1109/TAP.2003.822405, URL http://ieeexplore.ieee.org/document/1268323/.

[17] M. Camacho, R.R. Boix, F. Medina, Computationally efficient analysis of extraordinary optical transmission through infinite and truncated subwavelength hole arrays, Phys. Rev. E 93 (6) (2016) 063312, http://dx.doi.org/10.1103/PhysRevE.93.063312, URL http://link.aps.org/doi/10.1103/PhysRevE.93.063312.

[18] M. Camacho, R.R. Boix, F. Medina, A.P. Hibbins, J.R. Sambles, Theoretical and experimental exploration of finite sample size effects on the propagation of surface waves supported by slot arrays, Phys. Rev. B 95 (24) (2017) 245425, http://dx.doi.org/10.1103/PhysRevB.95.245425, URL http://link.aps.org/doi/10.1103/PhysRevB.95.245425.

[19] B.A. Munk, Finite Antenna Arrays and FSS, Wiley Interscience, Hoboken (New Jersey), USA, 2003.

[20] M. Camacho, R.R. Boix, F. Medina, Comparative study between resonant transmission and extraordinary transmission in truncated periodic arrays of slots, in: 2017 IEEE MTT-S International Conference on Numerical Electromagnetic and Multiphysics Modeling and Optimization for RF, Microwave, and Terahertz Applications (NEMO), IEEE, 2017, pp. 257–259, http://dx.doi.org/10.1109/NEMO.2017.7964252, URL http://ieeexplore.ieee.org/document/7964252/.

[21] T.W. Ebbesen, H.J. Lezec, H.F. Ghaemi, T. Thio, P.A. Wolff, Extraordinary optical transmission through sub-wavelength hole arrays, Nature 391 (6668) (1998) 667–669, URL http://dx.doi.org/10.1038/35570.

[22] B. Munk, D. Janning, J. Pryor, R. Marhefka, Scattering from surface waves on finite FSS, IEEE Trans. Antennas and Propagation 49 (12) (2001) 1782–1793, http://dx.doi.org/10.1109/8.982461, URL http://ieeexplore.ieee.org/document/982461/.

[23] D. Janning, B. Munk, Effects of surface waves on the currents of truncated periodic arrays, IEEE Trans. Antennas and Propagation 50 (9) (2002) 1254–1265, http://dx.doi.org/10.1109/TAP.2002.801378, URL http://ieeexplore.ieee.org/document/1048999/.

[24] Ö.A. Civi, P.H. Pathak, Array guided surface waves on a finite planar array of dipoles with or without a grounded substrate, IEEE Trans. Antennas and Propagation 54 (8) (2006) 2244–2252, http://dx.doi.org/10.1109/TAP.2006.879185, URL http://ieeexplore.ieee.org/document/1668298/.

[25] C. Cutler, Genesis of the corrugated electromagnetic surface, in: Proceedings of IEEE Antennas and Propagation Society International Symposium and URSI National Radio Science Meeting, Vol. 3, 1994, pp. 1456–1459, http://dx.doi.org/10.1109/APS.1994.408225, URL http://ieeexplore.ieee.org/document/408225/ http://ieeexplore.ieee.org/lpdocs/epic03/wrapper.htm?arnumber=408225.

[26] D.R. Jackson, J. Chen, R. Qiang, F. Capolino, A.A. Oliner, The role of leaky plasmon waves in the directive beaming of light through a subwavelength aperture, Opt. Express 16 (26) (2008) 21271–21281, http://dx.doi.org/10.1364/OE.16.021271, URL https://www.osapublishing.org/oe/abstract.cfm?uri=oe-16-26-21271.

[27] S. Maci, G. Minatti, M. Casaletti, M. Bosiljevac, Metasurfing: Addressing waves on impenetrable metasurfaces, IEEE Antennas Wirel. Propag. Lett. 10 (2011) 1499–1502, http://dx.doi.org/10.1109/LAWP.2012.2183631, URL http://ieeexplore.ieee.org/document/6127895/.

[28] D.R. Jackson, P. Burghignoli, G. Lovat, F. Capolino, J. Chen, D.R. Wilton, A.A. Oliner, The fundamental physics of directive beaming at microwave and optical frequencies and the role of leaky waves, Proc. IEEE 99 (10) (2011) 1780–1805, http://dx.doi.org/10.1109/JPROC.2010.2103530, URL http://ieeexplore.ieee.org/document/5771967/.

[29] D.R. Jackson, C. Caloz, T. Itoh, Leaky-wave antennas, Proc. IEEE 100 (7) (2012) 2194–2206, http://dx.doi.org/10.1109/JPROC.2012.2187410, URL http://ieeexplore.ieee.org/document/6174425/.

[30] C. Pfeiffer, A. Grbic, A. printed, A printed broadband luneburg lens antenna, IEEE Trans. Antennas and Propagation 58 (9) (2010) 3055–3059, http://dx.doi.org/10.1109/TAP.2010.2052582, URL http://ieeexplore.ieee.org/document/5484658/.

[31] M. Camacho, R.C. Mitchell-Thomas, A.P. Hibbins, J. Roy Sambles, O. Quevedo-Teruel, Designer surface plasmon dispersion on a one-dimensional periodic slot metasurface with glide symmetry, Opt. Lett. 42 (17) (2017) 3375, http://dx.doi.org/10.1364/OL.42.003375, URL https://www.osapublishing.org/abstract.cfm?URI=ol-42-17-3375.

[32] M. Camacho, R.C. Mitchell-Thomas, A.P. Hibbins, J.R. Sambles, O. Quevedo-Teruel, Mimicking glide symmetry dispersion with coupled slot metasurfaces, Appl. Phys. Lett. 111 (12) (2017) 121603, http://dx.doi.org/10.1063/1.5000222, URL http://dx.doi.org/10.1063/1.5000222.

[33] B. Noble, Methods Based on the Wiener–Hopf Technique, Pergamon, London, 1958, URL https://books.google.co.uk/books/about/Methods{_}Based{_}on{_}the{_}Wiener{_}Hopf{_}Techniq.html?id=eLnPm6Eid7oC http://books.google.com/books?hl=en&lr=&id=hvVsGo8eo9UC&oi=fnd&pg=PP11&dq=Methods+Based+on+the+Wiener--Hopf+Technique+for+the+Solution+.

[34] R. Mittra, S.W. Lee, Analytical Techniques in the Theory of Guided Waves, Macmillan, New York, 1971, URL https://books.google.co.uk/books?id=R-c8AAAAIAAJ.

[35] F. Capolino, M. Albani, Truncation effects in a semi-infinite periodic array of thin strips: A discrete Wiener–Hopf formulation, Radio Sci. 44 (2) (2009) 1–14, http://dx.doi.org/10.1029/2007RS003821, URL http://doi.wiley.com/10.1029/2007RS003821.
[36] I.N. Fel'd, Diffraction of electromagnetic waves on a semi-infinite grating, Radiotekh. Electron. 3 (1958) 882–888.
[37] N.L. Hills, S.N. Karp, Semi-infinite diffraction gratings-i *, Comm. Pure Appl. Math. XVIII (1965) 203–233.
[38] W. Wasylkiwskyj, Mutual coupling effects in semi-infinite arrays, IEEE Trans. Antennas and Propagation 21 (3) (1973) 277–285, http://dx.doi.org/10.1109/TAP.1973.1140507, URL http://ieeexplore.ieee.org/document/1140507/ http://ieeexplore.ieee.org/xpls/abs_all.jsp?arnumber=1140507.
[39] A.L. VanKoughnett, Mutual coupling effects in linear antenna arrays, Can. J. Phys. 48 (6) (1970) 659–674, http://dx.doi.org/10.1139/p70-085, URL http://www.nrcresearchpress.com/doi/10.1139/p70-085.
[40] M. Albani, F. Capolino, Wave dynamics by a plane wave on a half-space metamaterial made of plasmonic nanospheres: a discrete Wiener–Hopf formulation, J. Opt. Soc. Amer. B 28 (9) (2011) 2174, http://dx.doi.org/10.1364/JOSAB.28.002174, URL https://www.osapublishing.org/abstract.cfm?URI=josab-28-9-2174.
[41] N. Tymis, I. Thompson, Low-frequency scattering by a semi-infinite lattice of cylinders, Quart. J. Mech. Appl. Math. 64 (2) (2011) 171–195, http://dx.doi.org/10.1093/qjmam/hbr001, URL https://academic.oup.com/qjmam/article-lookup/doi/10.1093/qjmam/hbr001.
[42] Y. Hadad, B.Z. Steinberg, Green's function theory for infinite and semi-infinite particle chains, Phys. Rev. B 84 (12) (2011) 125402, http://dx.doi.org/10.1103/PhysRevB.84.125402, URL https://link.aps.org/doi/10.1103/PhysRevB.84.125402.
[43] P.A. Martin, I.D. Abrahams, W.J. Parnell, One-dimensional reflection by a semi-infinite periodic row of scatterers, Wave Motion 58 (2015) 1–12, http://dx.doi.org/10.1016/j.wavemoti.2015.06.005, URL https://www.sciencedirect.com/science/article/pii/S0165212515000931.
[44] R.F. Harrington, Field Computation By Moment Methods, Wiley-IEEE Press, New York, USA, 1993.
[45] R. Rodriguez-Berral, F. Mesa, F. Medina, Analytical multimodal network approach for 2-d arrays of planar patches/apertures embedded in a layered medium, IEEE Trans. Antennas and Propagation 63 (5) (2015) 1969–1984, http://dx.doi.org/10.1109/TAP.2015.2406885.
[46] S.R. Rengarajan, Choice of basis functions for accurate characterization of infinite array of microstrip reflectarray elements, IEEE Antennas Wirel. Propag. Lett. 4 (2005) 47–50.
[47] R. Boix, M. Freire, F. Medina, New method for the efficient summation of double infinite series arising from the spectral domain analysis of frequency selective surfaces, IEEE Trans. Antennas and Propagation 52 (4) (2004) 1080–1094, http://dx.doi.org/10.1109/TAP.2004.825671, URL http://ieeexplore.ieee.org/document/1291773/.
[48] K.E. Jordan, G.R. Richter, P. Sheng, An efficient numerical evaluation of the green's function for the helmholtz operator on periodic structures, J. Comput. Phys. 63 (1) (1986) 222–235, http://dx.doi.org/10.1016/0021-9991(86)90093-8, URL http://linkinghub.elsevier.com/retrieve/pii/0021999186900938.
[49] G. Valerio, P. Baccarelli, P. Burghignoli, A. Galli, Comparative analysis of acceleration techniques for 2-D and 3-D Green's functions in periodic structures along one and two directions, IEEE Trans. Antennas and Propagation 55 (6 I) (2007) 1630–1643, http://dx.doi.org/10.1109/TAP.2007.897340, URL http://ieeexplore.ieee.org/document/4232656/.
[50] F.T. Celepcikay, D.R. Wilton, D.R. Jackson, F. Capolino, Choosing splitting parameters and summation limits in the numerical evaluation of 1-D and 2-D periodic green's functions using the ewald method, Radio Sci. 43 (5) (2008) http://dx.doi.org/10.1029/2007RS003820, n/a–n/a.
[51] R. Florencio, R.R. Boix, J.A. Encinar, Enhanced MoM analysis of the scattering by periodic strip gratings in multilayered substrates, IEEE Trans. Antennas and Propagation 61 (10) (2013) 5088–5099, http://dx.doi.org/10.1109/TAP.2013.2273213, URL http://ieeexplore.ieee.org/document/6558474/.
[52] V. Galdi, I.M. Pinto, Simple algorithm for accurate location of leaky-wave poles for grounded inhomogeneous dielectric slabs, Microw. Opt. Technol. Lett. 24 (2) (2000) 135–140, http://dx.doi.org/10.1002/(SICI)1098-2760(20000120)24:2<135::AID-MOP17>3.0.CO;2-P, URL http://doi.wiley.com/10.1002/%28SICI%291098-2760%2820000120%2924%3A2%3C135%3A%3AAID-MOP17%3E3.0.CO%3B2-P.
[53] M. Camacho, R.R. Boix, F. Medina, A.P. Hibbins, J.R. Sambles, On the extraordinary optical transmission in parallel plate waveguides for non-TEMmodes, Opt. Express 25 (20) (2017) 24670, http://dx.doi.org/10.1364/OE.25.024670, URL https://www.osapublishing.org/abstract.cfm?URI=oe-25-20-24670.
[54] M. Camacho, A.P. Hibbins, J.R. Sambles, Resonantly induced transparency for metals with low angular dependence, Appl. Phys. Lett. 109 (24) (2016) 241601, http://dx.doi.org/10.1063/1.4971983, URL http://scitation.aip.org/content/aip/journal/apl/109/24/10.1063/1.4971983.